Springer

Journal of Mechanical Science and Technology 23 (2009) 358~371

Journal of
Mechanical
Science and
Technology

www.springerlink.com/content/1738-494x
DOI 10.1007/s12206-008-1008-2

Vibration of two cantilever beams clamped at one end and connected by a rigid body at the other †

Kyung Taek Lee*

LG Electronics Inc. 16 Woomyeon-Dong, Seocho-Gu, 137-140 Seoul, Korea

(Manuscript Received June 4, 2008; Revised October 13, 2008; Accepted October 26, 2008)

Abstract

This study presents the pure bending and coupled bending-torsional vibration characteristics of a beam structure which consists of two cantilever beams and a rigid body at their free ends. This structure is available in many mechanical structures such as robots, space constructions, and optical pickup actuators in optical disc drives (ODDs). In order to depict the vibration of the beam structure originating from the deflection and torsion of two beams, the motion equations and continuity conditions are analytically induced by using energy conservation. In the process that the free vibration problem is solved, two independent characteristic equations are obtained. The former is an equation for the pure bending vibration of two beams, and the latter is for their coupled bending-torsional vibration. It is proved that these characteristic equations are exact by comparing natural frequencies obtained from FEM. As natural frequencies are described in many dimensional variations, the relation between vibration characteristics and the dimensions of the given system is also investigated. Finally, resonant frequencies from test results are presented to confirm the validation of this study for a new type optical pickup actuator.

Keywords: Beam; Natural frequency; Characteristic equation; Pure bending vibration; Coupled bending-torsional vibration

1. Introduction

Over the years, a large number of studies have been conducted to explain the dynamic characteristics of beam structures. The studies mainly focus on the analysis of dynamic behaviors about a single beam with a tip mass under various boundary conditions, a beam with non-uniform sections such as a stepped beam, and a multi-beam structure.

Gurgoze and Batan treated the vibrations of a restrained cantilever beam carrying a heavy tip body [1]. Farghaly presented the vibration characteristics of an axially loaded cantilever beam with an elastically mounted end mass [2]. Jang and Bert solved the free vibration problems of a stepped beam under various boundary conditions [3]. Rossi and Laura obtained natural frequencies in a cantilever with non-uniform thickness and a tip mass [4]. Auciello introduced the solution of a vibration problem in a linearly tapered cantilever beam having the eccentricity of an end mass [5]. The coupling effect between bending and torsional vibrations on the natural frequencies and modes was explained by Dokumaci [6]. Exact frequency equation and mode shape expressions for a coupled bending-torsional beam with cantilever end condition were derived by Banerjee [7]. As treating the coupling effect of a beam, Gökdağ and Kopmaz examined the coupled flexural-torsional free and forced vibrations of a beam with several tip attachments [8]. Anderson expanded the subject for a simple beam into that for a multi-beam structure and solved the coupled bending-longitudinal vibration problem of two parallel and uniform beams connected by a rigid body with its mass and mass moment of

† This paper was recommended for publication in revised form by Associate Editor Eung-Soo Shin

*Corresponding author. Tel.: +82 2 526 4757, Fax.: +82 2 526 4758
E-mail address: lkt@lge.cm / leektaek@naver.com

inertia [9]. His result shows that natural frequencies and modes are affected by the geometrical coupling and dimensional parameters. Kwon et al. improved Anderson's model into a stepped beam structure and showed that natural frequencies were changed by various beam conditions [10].

In this paper, vibration characteristics of two beams caused by a connected rigid body are analyzed. Two beams are assumed to be uniform and sufficiently slender to ignore their shear deformations and rotary inertias in lateral directions. For making a mathematical model for this system, kinetic and potential energies are induced and energy conservative law are used. As boundary and joint conditions are applied to the mathematical model, the equations of motion and continuity conditions at the free ends of two beams are acquired. In the process that solves induced boundary value problems, two characteristic equations that can yield natural frequencies and modes for this beam structure are obtained. This paper shows that dynamic behaviors described by the characteristic equations accord with the pure bending (two beams are deflected equally and simultaneously.) and coupled bending-torsional vibrations of two beams with a rigid body at their free ends, respectively. By simulating the vibration characteristics of this system by FE analysis and comparing them with those of this study, it is proved that the characteristic equations explain the pure bending and coupled motions of beams. By changing dimensions in this system, the variations of fundamental natural frequencies are also explored and analyzed to understand the dynamic characteristics. Finally, resonant frequencies are measured by a real test and these are compared with the values from the exact solution of this study. It is shown that the vibration characteristics of a new type actuator can be expressed by this work.

2. Research motivation

Optical pickups, which are used in ODDs, are components to read and write information data on an optical disc such as CD, DVD and Blu-ray disc. In the optical pickup, the laser is focused on a rotating disc to read and write the information by an objective lens (OL). A real plastic disc has various deflections occurring in the manufacturing process and is mounted with a skew angle on a spindle motor. Therefore, the OL moves along the perpendicular direction to the disc surface and along the direction crossing the data track for focusing and tracking controls of the laser spot to accurately follow the disc displacement. The driving mechanism of this OL is the optical pickup actuator. Conventional actuators include a moving part and a fixed part. The moving part, which has a lens-holder, coils and the OL, is suspended by four or six wire-suspensions as shown in Fig. 1. In general, the diameter of the wire-suspension is 0.1mm or less. The moving part rotates a small angle around an axis parallel to the wire-suspension and moves to the focusing and tracking directions.

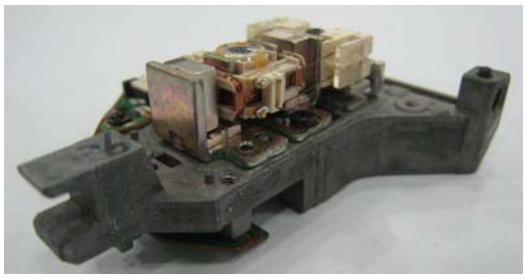

Fig. 1. Conventional optical pickup actuator with four wire-suspensions.

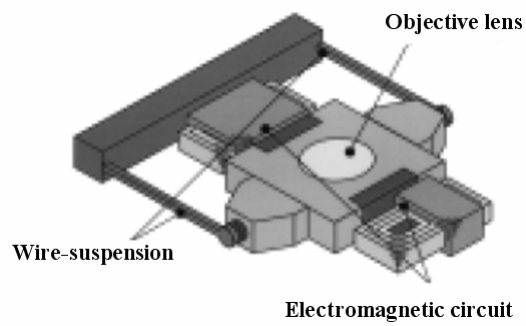

(a) Configuration of new type 4-axis actuator

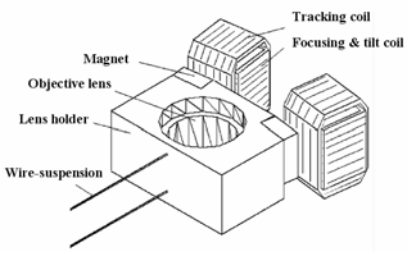

(b) Configuration of new type 3-axis actuator

Fig. 2. Optical pickup actuators with two wire-suspensions.

Recent researches in ODDs, which have focused on high density and high data capacity [11, 12], require the control of a quite large tilt angle in the actuator. There are several studies on actuators satisfying this requirement. Motegi et al. introduced a 4-axis actuator to achieve two tilt controls and He et al. proposed a new type of 3-axis actuator shown in Figs. 2-a, 2-b [13, 14]. These actuators have two wire-suspensions to get high flexibility in the radial tilt direction or/and tangential tilt direction. Although the controllability of these three-axis and four-axis actuators is not better than conventional types, the merits obtained by their simple and slim structures are expected to raise the usability of two wire-suspension type actuator in next generation ODDs such as near-field recording systems [11, 12].

Although FE analysis is widely used in the analysis of mechanical systems, mathematical analysis is treated as a useful tool because the decision of basic design specifications and the modification of design are easily achieved. For the analysis of a two wire-suspension type actuator, Anderson's study can be used to describe the lateral vibration (in-plane motion) of the actuator as a coupled axial-bending motion is considered [9]. The lateral vibration analysis can express focusing, tracking, pitching, and yawing mode vibrations in the two wire-suspension type actuator. However, there are no other studies on coupled bending-torsional vibration to characterize the rotating vibration of the actuator. This paper aims to describe the vibration characteristics for rotating motion as the coupled bending-torsional vibration for a two-beam structure is mathematically analyzed.

3. Mathematical formulation

Two uniform cantilevers joined by a rigid body at their free ends are shown in Fig. 3. Two beams are slender and uniform so that their shear deformations and rotary inertias in lateral directions can be ignored. In order to depict the motion of the rigid body caused by bending and torsional vibrations of two beams, it is assumed that the beams are deflectable along the x_2 direction and rotatable around the x_1 axis. On the other hand, longitudinal deformation in the x_1 direction and deflection along the x_3 direction are not considered. Therefore rotation angles $\phi_1(x_1,t), \phi_2(x_1,t)$ around the x_1 axis and lateral deflections $v_1(x_1,t), v_2(x_1,t)$ of x_2 direction in two beams should be considered to describe the motion of this system.

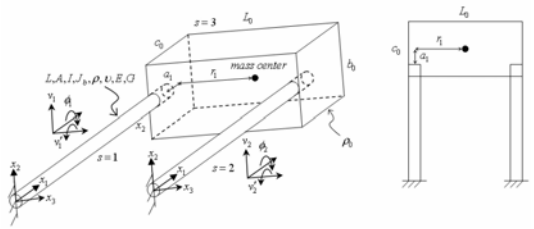

Fig. 3 Two uniform cantilever beams connected by a rigid body.

By simple-beam theory [15], this system has the following boundary conditions at their fixed ends.

$$\phi_s(x_1,t) = v_s(x_1,t) = v_s'(x_1,t) = 0 \quad \text{at} \quad x_1 = 0\,, \quad s = 1,2\,, \tag{1}$$

where, $v_s'(x_1,t) = \dfrac{\partial v_s(x_1,t)}{\partial x_1}$ denotes lateral deflection angle, s designates each beam, t is time. In addition, the joint conditions at $x_1 = L$ are

$$\begin{aligned} &\phi_1(L,t) = \phi_2(L,t)\,, \quad v_1'(L,t) = v_2'(L,t)\,, \\ &v_2(L,t) = v_1(L,t) - 2r_1\phi_1(L,t)\,, \end{aligned} \tag{2}$$

where, r_1 is the distance along x_3 axis from the free end of the beam($s = 1$) to the mass center of the rigid body.

The kinetic and potential(strain) energies of each beam are expressed as

$$T_s = \int_0^L \left[\frac{1}{2}\rho J_b \dot{\phi}_s^2(x_1,t) + \frac{1}{2}\rho A \dot{v}_s^2(x_1,t) \right] dx_1\,, \quad s = 1,2\,, \tag{3}$$

$$V_s = \int_0^L \left[\frac{1}{2} G J_b \phi_s'^2(x_1,t) + \frac{1}{2} E I v_s''^2(x_1,t) \right] dx_1\,, \quad s = 1,2\,, \tag{4}$$

where, L denotes the length of the beam, ρ its density, E the modulus of elasticity, G the modulus of elasticity in shear, A the cross-sectional area, I the area moment of inertia, J_b the polar moment of inertia, $\phi_s'(x_1,t) = \dfrac{\partial \phi_s(x_1,t)}{\partial x_1}$, $\dot{\phi}_s(x_1,t) = \dfrac{\partial \phi_s(x_1,t)}{\partial t}$, $\dot{v}_s(x_1,t) = \dfrac{\partial v_s(x_1,t)}{\partial t}$, etc. In Eq. (3), the rotary inertia term for the beam is neglected. The potential energy of the rigid body is not considered in this paper. Its kinetic energy is

$$T_3 = \frac{1}{2}m\left\{\dot{v}_1(L,t) + a_1\dot{v}_1'(L,t) - r_1\dot{\phi}_1(L,t)\right\}^2 + \frac{1}{2}J_1\dot{\phi}_1^2(L,t) + \frac{1}{2}J_2\dot{v}_1'^2(L,t) \quad , \tag{5}$$

where, m is the mass of the rigid body, a_1 the distance between the free end of the 1st beam and the mass center of the rigid body along x_1 axis, $J_1 = \frac{m}{12}\left(b_0^2 + L_0^2\right)$ and $J_2 = \frac{m}{12}\left(b_0^2 + c_0^2\right)$ the mass moments of inertia defined at its mass center. The mass and mass moments of inertia can be expressed as follows.

$$m = \rho_0 b_0 c_0 L_0 \ , \ J_1 = mh_1^2 \ , \ J_2 = mk_1^2 \ , \tag{6}$$

where, ρ_0 is the density of the rigid body, L_0 its width, b_0 its height, c_0 its length, $h_1 = \sqrt{\left(b_0^2 + L_0^2\right)/12}$ and $k_1 = \sqrt{\left(b_0^2 + c_0^2\right)/12}$ the radii of gyration of the rigid body, respectively. Unfolding Eq. (5),

$$T_3 = \left[\frac{1}{2}m\dot{v}_1^2 + \frac{1}{2}mh_1^2\dot{\phi}_1^2 + \frac{1}{2}mk_1^2\dot{v}_1'^2 + \frac{1}{2}ma_1^2\dot{v}_1'^2 + \frac{1}{2}mr_1^2\dot{\phi}_1^2 + ma_1\dot{v}_1\dot{v}_1' - ma_1r_1\dot{v}_1'\dot{\phi}_1 - mr_1\dot{v}_1\dot{\phi}_1\right]_{x_1=L} \quad , \tag{7}$$

where, $\phi_1 = \phi_1(x_1,t)$ and $v_1 = v_1(x_1,t)$. The kinetic energy of the whole system is

$$\sum_{j=1}^{3}T_j = \sum_{s=1}^{2}T_s + T_3 = \sum_{s=1}^{2}\int_0^L\left[\frac{1}{2}\rho J_b\dot{\phi}_s^2(x_1,t) + \frac{1}{2}\rho A\dot{v}_s^2(x_1,t)\right]dx_1 + \left[\frac{1}{2}m\dot{v}_1^2 + \frac{1}{2}mh_1^2\dot{\phi}_1^2 + \frac{1}{2}mk_1^2\dot{v}_1'^2 + \frac{1}{2}ma_1^2\dot{v}_1'^2 + \frac{1}{2}mr_1^2\dot{\phi}_1^2 + ma_1\dot{v}_1\dot{v}_1' - ma_1r_1\dot{v}_1'\dot{\phi}_1 - mr_1\dot{v}_1\dot{\phi}_1\right]_{x_1=L} . \tag{8}$$

Similarly, the potential energy is

$$\sum_{j=1}^{3}V_j = \sum_{s=1}^{2}V_s = \sum_{s=1}^{2}\int_0^L\left[\frac{1}{2}GJ_b\phi_s'^2(x_1,t) + \frac{1}{2}EIv_s''^2(x_1,t)\right]dx_1 \ . \tag{9}$$

According to the energy conservation law, the total energy of the system is time-invariant.

$$\frac{\partial}{\partial t}\left(\sum_{j=1}^{3}T_j + \sum_{j=1}^{3}V_j\right) = \sum_{j=1}^{3}\frac{\partial}{\partial t}T_j + \sum_{j=1}^{3}\frac{\partial}{\partial t}V_j = 0 \ . \tag{10}$$

For obtaining each term of the above, one calculates the time derivative of the kinetic energy.

$$\sum_{j=1}^{3}\frac{\partial}{\partial t}T_j = \sum_{s=1}^{2}\int_0^L\left[\rho J_b\dot{\phi}_s\ddot{\phi}_s + \rho A\dot{v}_s\ddot{v}_s\right]dx_1 + \left[m\dot{v}_1\ddot{v}_1 + mh_1^2\dot{\phi}_1\ddot{\phi}_1 + mk_1^2\dot{v}_1'\ddot{v}_1' + ma_1^2\dot{v}_1'\ddot{v}_1' + mr_1^2\dot{\phi}_1\ddot{\phi}_1 + ma_1\ddot{v}_1\dot{v}_1' + ma_1\dot{v}_1\ddot{v}_1' - ma_1r_1\ddot{v}_1'\dot{\phi}_1 - ma_1r_1\dot{v}_1'\ddot{\phi}_1 - mr_1\ddot{v}_1\dot{\phi}_1 - mr_1\dot{v}_1\ddot{\phi}_1\right]_{x_1=L} , \tag{11}$$

where, $\phi_s = \phi_s(x_1,t)$ and $v_s = v_s(x_1,t)$. The time derivative of the potential energy is also

$$\sum_{j=1}^{3}\frac{\partial}{\partial t}V_j = \sum_{s=1}^{2}\frac{\partial}{\partial t}V_s = \sum_{s=1}^{2}\int_0^L\left[GJ_b\phi_s'\dot{\phi}_s' + EIv_s''\dot{v}_s''\right]dx_1 \ . \tag{12}$$

Integration by parts yields

$$\sum_{s=1}^{3}\frac{\partial}{\partial t}V_j = \sum_{s=1}^{2}\left[\left|GJ_b\phi_s'\dot{\phi}_s\right|_0^L - \int_0^L GJ_b\phi_s''\dot{\phi}_s\,dx_1\right] + \sum_{s=1}^{2}\left[\left|EIv_s''\dot{v}_s'\right|_0^L - \left|EIv_s'''\dot{v}_s\right|_0^L + \int_0^L EIv_s^{(4)}\dot{v}_s\,dx_1\right] , \tag{13}$$

where, $v_s^{(4)} = \frac{\partial^4 v_s(x_1,t)}{\partial x_1^4}$. Inserting conditions (1) and (2) into Eq. (13) gives us

$$\sum_{j=1}^{3}\frac{\partial}{\partial t}V_j = \sum_{s=1}^{2}\int_0^L\left(-GJ_b\phi_s''\dot{\phi}_s + EIv_s^{(4)}\dot{v}_s\right)dx_1 + \left[GJ_b\phi_1'\dot{\phi}_1 + GJ_b\phi_2'\dot{\phi}_1 + EIv_1''\dot{v}_1' + EIv_2''\dot{v}_1' - EIv_1'''\dot{v}_1 - EIv_2'''(\dot{v}_1 - 2r_1\dot{\phi}_1)\right]_{x_1=L} . \tag{14}$$

Inserting Eqs. (11) and (14) into Eq. (10) makes

$$\sum_{s=1}^{2}\int_0^L(\rho J_b\ddot{\phi}_s - GJ_b\phi_s'')\dot{\phi}_s dx_1 + \sum_{s=1}^{2}\int_0^L(\rho A\ddot{v}_s + EIv_s^{(4)})\dot{v}_s dx_1 + [(m\ddot{v}_1 + ma_1\ddot{v}_1' - mr_1\ddot{\phi}_1 - EIv_1''' - EIv_2''')\dot{v}_1 + \{m(h_1^2 + r_1^2)\ddot{\phi}_1 - ma_1r_1\ddot{v}_1' - mr_1\ddot{v}_1 + 2r_1EIv_2''' + GJ_b\phi_1' + GJ_b\phi_2'\}\dot{\phi}_1 + \{m(k_1^2 + a_1^2)\ddot{v}_1' + ma_1\ddot{v}_1 - ma_1r_1\ddot{\phi}_1 + EIv_1'' + EIv_2''\}\dot{v}_1']_{x_1=L} = 0 . \tag{15}$$

From the condition that the above equation is always zero, motion Eqs. (16), (17) and continuity conditions (18)-(20) at $x_1 = L$ are obtained.

$$\rho\ddot{\phi}_s(x_1,t) - G\phi_s''(x_1,t) = 0, \quad 0 < x_1 < L\ , \quad 0 < t\ , \quad s = 1,2\ , \tag{16}$$

$$\rho A\ddot{v}_s(x_1,t) + EIv_s^{(4)}(x_1,t) = 0\ , \quad 0 < x_1 < L\ , \quad 0 < t\ , \quad s = 1,2\ , \tag{17}$$

$$\left[m\ddot{v}_1 + ma_1\ddot{v}_1' - mr_1\ddot{\phi}_1 - EIv_1''' - EIv_2'''\right]_{x_1=L} = 0\ , \tag{18}$$

$$\left[m(h_1^2 + r_1^2)\ddot{\phi}_1 - ma_1r_1\ddot{v}_1' - mr_1\ddot{v}_1 + 2r_1EIv_2''' + GJ_b\phi_1' + GJ_b\phi_2'\right]_{x_1=L} = 0\ , \tag{19}$$

$$\left[m(k_1^2 + a_1^2)\ddot{v}_1' + ma_1\ddot{v}_1 - ma_1r_1\ddot{\phi}_1 + EIv_1'' + EIv_2''\right]_{x_1=L} = 0\ . \tag{20}$$

4. Normalized expressions

To make forms normalized by time and beam length L and simplify the above equations, one sets

$$\varphi_s(x_1,t) = L\phi_s(x_1,t)\ , \quad s = 1,2\ , \tag{21}$$

$$x = x_1/L, \quad \tau = t/\sigma, \quad \sigma^2 = \rho L^2/G, \quad \mu = m/\rho AL, \quad \alpha^2 = EI/GAL^2, \quad \zeta = GJ_b/EI, \quad a = a_1/L, \quad r = r_1/L, \quad h = h_1/L, \quad k = k_1/L, \tag{22}$$

where, x and τ are the non-dimensional coordinate and time, respectively. Using Eqs. (21) and (22), the normalized forms of Eqs. (1), (2) and (16)-(20) become

$$\varphi_s''(x,\tau) - \ddot{\varphi}_s(x,\tau) = 0\ , \quad 0 < x < 1\ , \quad 0 < \tau\ , \quad s = 1,2\ , \tag{23}$$

$$\alpha^2 v_s^{(4)}(x,\tau) + \ddot{v}_s(x,\tau) = 0\ , \quad 0 < x < 1\ , \quad 0 < \tau\ , \quad s = 1,2\ , \tag{24}$$

$$\varphi_s(0,\tau) = v_s(0,\tau) = v_s'(0,\tau) = 0\ , \tag{25}$$

$$\varphi_1(1,\tau) = \varphi_2(1,\tau)\ , \quad v_1'(1,\tau) = v_2'(1,\tau)\ , \quad v_2(1,\tau) = v_1(1,\tau) - 2r\varphi_1(1,\tau)\ , \tag{26}$$

$$\mu\ddot{v}_1(1,\tau) + \mu a\ddot{v}_1'(1,\tau) - \mu r\ddot{\varphi}_1(1,\tau) - \alpha^2 v_1'''(1,\tau) - \alpha^2 v_2'''(1,\tau) = 0\ , \tag{27}$$

$$\mu(h^2 + r^2)\ddot{\varphi}_1(1,\tau) - \mu ar\ddot{v}_1'(1,\tau) - \mu r\ddot{v}_1(1,\tau) + 2r\alpha^2 v_2'''(1,\tau) + \zeta\alpha^2\varphi_1'(1,\tau) + \zeta\alpha^2\varphi_2'(1,\tau) = 0\ , \tag{28}$$

$$\mu(k^2 + a^2)\ddot{v}_1'(1,\tau) + \mu a\ddot{v}_1(1,\tau) - \mu ar\ddot{\varphi}_1(1,\tau) + \alpha^2 v_1''(1,\tau) + \alpha^2 v_2''(1,\tau) = 0\ , \tag{29}$$

where, $\varphi_s' = \partial\varphi_s/\partial x$, $\dot{\varphi}_s = \partial\varphi_s/\partial\tau$, $v_s' = \partial v_s/\partial x$, $\dot{v}_s = \partial v_s/\partial\tau$, and etc.

5. Free motion problems

In synchronous motion systems, the solutions of motion equations can be separately expressed as the functions of space and time. The solutions of differential Eqs. (23) and (24) can be assumed to be

$$\varphi_s(x,\tau) = \varphi_s(x)\cos\omega_n\tau\ , \quad v_s(x,\tau) = v_s(x)\cos\omega_n\tau\ , \quad s = 1,2\ , \tag{30}$$

where, ω_n is normalized natural radian frequency. To make these equations simpler, the following expression is used.

$$\lambda^2 = \omega_n/\alpha\ . \tag{31}$$

Using Eqs. (30) and (31), one can convert Eqs. (23)-(29) to the following equations.

$$\varphi_s''(x) + \omega_n^2\varphi_s(x) = 0\ , \quad s = 1,2\ , \tag{32}$$

$$v_s^{(4)}(x) - \lambda^4 v_s(x) = 0\ , \quad s = 1,2\ , \tag{33}$$

$$\varphi_s(0) = v_s(0) = v_s'(0) = 0\ , \tag{34}$$

$$\varphi_1(1) = \varphi_2(1)\ , \quad v_1'(1) = v_2'(1)\ , \quad v_2(1) = v_1(1) - 2r\varphi_1(1)\ , \tag{35}$$

$$\mu\omega_n^2 v_1(1) + \mu a\omega_n^2 v_1'(1) - \mu r\omega_n^2\varphi_1(1) + \alpha^2 v_1'''(1) + \alpha^2 v_2'''(1) = 0\ , \tag{36}$$

$$\mu(h^2 + r^2)\omega_n^2\varphi_1(1) - \mu ar\omega_n^2 v_1'(1) - \mu r\omega_n^2 v_1(1) - 2r\alpha^2 v_2'''(1) - \zeta\alpha^2\varphi_1'(1) - \zeta\alpha^2\varphi_2'(1) = 0\ , \tag{37}$$

$$\mu(k^2 + a^2)\omega_n^2 v'(1) + \mu a\omega_n^2 v_1(1) - \mu ar\omega_n^2\ddot{\varphi}_1(1) - \alpha^2 v_1''(1) - \alpha^2 v_2''(1) = 0\ . \tag{38}$$

The solutions of the boundary value problem, satisfying boundary conditions (34), are

$$\varphi_s(x) = B_s\sin\omega_n x\ , \quad s = 1,2\ , \tag{39}$$

$$v_s(x) = C_s(\cos\lambda x - \cosh\lambda x) + D_s(\sin\lambda x - \sinh\lambda x)\ , \quad s = 1,2\ , \tag{40}$$

where, B_1, B_2, C_1, D_1, C_2 and D_2 are modal coefficients. $B_1 = B_2$ is apparent by the first condition $\varphi_1(1) = \varphi_2(1)$ in conditions (35). Insertion of Eqs. (39) and (40) to Eqs. (35)-(38) to obtain other coefficients yields the following matrix form.

$$\left[a_{ij}\right]\{b_j\} = \{0\}, \quad i,j = 1,2,3,4,5\ . \tag{41}$$

The components of matrix $\left[a_{ij}\right]$ are as follows.

$a_{11}=0$, $a_{12}=s+sh$, $a_{13}=-(c-ch)$,
$a_{14}=-(s+sh)$, $a_{15}=c-ch$,
$a_{21}=2r\sin\omega_n$, $a_{22}=-(c-ch)$, $a_{23}=-(s-sh)$,
$a_{24}=c-ch$, $a_{25}=s-sh$,
$a_{31}=\mu r\omega_n^2\sin\omega_n$,
$a_{32}=-\mu\omega_n^2(c-ch)+\mu a\omega_n^2\lambda(s+sh)-\alpha^2\lambda^3(s-sh)$,
$a_{33}=-\mu\omega_n^2(s-sh)-\mu a\omega_n^2\lambda(c-ch)+\alpha^2\lambda^3(c+ch)$,
$a_{34}=-\alpha^2\lambda^3(s-sh)$, $a_{35}=\alpha^2\lambda^3(c+ch)$,
$a_{41}=-\mu(h^2+r^2)\omega_n^2\sin\omega_n+2\zeta\alpha^2\omega_n\cos\omega_n$,
$a_{42}=-\mu ar\omega_n^2\lambda(s+sh)+\mu r\omega_n^2(c-ch)$, (42)
$a_{43}=\mu ar\omega_n^2\lambda(c-ch)+\mu r\omega_n^2(s-sh)$,
$a_{44}=2r\alpha^2\lambda^3(s-sh)$, $a_{45}=-2r\alpha^2\lambda^3(c+ch)$,
$a_{51}=\mu ar\omega_n^2\sin\omega_n$,
$a_{52}=\mu(k^2+a^2)\omega_n^2\lambda(s+sh)-\mu a\omega_n^2(c-ch)-\alpha^2\lambda^2(c+ch)$,
$a_{53}=-\mu(k^2+a^2)\omega_n^2\lambda(c-ch)-\mu a\omega_n^2(s-sh)-\alpha^2\lambda^2(s+sh)$,
$a_{54}=-\alpha^2\lambda^2(c+ch)$, $a_{55}=-\alpha^2\lambda^2(s+sh)$,

where, $s+sh=\sin\lambda+\sinh\lambda$, $s-sh=\sin\lambda-\sinh\lambda$, $c+ch=\cos\lambda+\cosh\lambda$, and $c-ch=\cos\lambda-\cosh\lambda$. The modal vector is

$$\{b_j\}=\{B_1 \quad C_1 \quad D_1 \quad C_2 \quad D_2\}^T. \tag{43}$$

Making non-trivial the matrix equation leads to $\det[a_{ij}]=0$. Computer-aided mathematical software [16] is useful to solve this determinant. As a result, two independent characteristic equations are obtained.

$$\begin{aligned}&(k^2\mu^2\lambda^4+4)-[(k^2\mu^2\lambda^4-4)\cos\lambda+\\&2\mu\lambda(a^2\lambda^2+k^2\lambda^2+1)\sin\lambda]\cosh\lambda\\&-2\mu\lambda[(a^2\lambda^2+k^2\lambda^2-1)\cos\lambda+2a\lambda\sin\lambda]\sinh\lambda\\&=0,\end{aligned} \tag{44}$$

$$\begin{aligned}&(2\alpha\zeta\cos\omega_n-h^2\mu\lambda^2\sin\omega_n)(1-\cos\lambda\cosh\lambda)\\&+2\lambda r^2\sin\omega_n(\sin\lambda\cosh\lambda+\cos\lambda\sinh\lambda)=0\end{aligned}. \tag{45}$$

The characteristic Eqs. (44) and (45) yield an infinity of characteristic values leading to the associated natural modes. However, it should be noted that higher modes become increasingly inaccurate due to the limitations of simple-beam theory [17].

Eq. (44) is comparably similar to Eq. (8) in reference [18], which is the characteristic equation for the pure bending vibration of a uniform cantilever with a tip mass.

$$\begin{aligned}&1+\kappa\psi\eta^4+(1-\kappa\psi\eta^4)G(\eta)+\kappa\eta[H(\eta)-J(\eta)]\\&-\psi\eta^3[H(\eta)+J(\eta)]\\&-2\kappa\varepsilon\eta^2F(\eta)-\kappa\varepsilon^2\eta^3[H(\eta)+J(\eta)]\\&=0,\end{aligned} \tag{46}$$

where, $F(\eta)=\sinh\eta\sin\eta$, $G(\eta)=\cosh\eta\cos\eta$, $H(\eta)=\sinh\eta\cos\eta$, $J(\eta)=\cosh\eta\sin\eta$, $\eta=\sqrt[4]{\frac{m\omega^2}{EI}}L$, $\varepsilon=a_1/L$, $\kappa=M/mL$, $\psi=J_2/mL^3$, and $J_2=\frac{m}{12}\left(b_0^2+c_0^2\right)$. Although the system in this paper has two beams, it is reasonable to suppose that its pure bending vibration is identical with that of a uniform cantilever with a tip mass. Thus, it seems quite probable that Eq. (44) is a characteristic equation for the pure bending vibration of two beams connected by a rigid body. In order to confirm this point, the characteristic equation is obtained under the circumstance that lateral deflections $v_1(x_1,t)$, $v_2(x_1,t)$ are only allowed. In such a case, joint conditions (35) are replaced by the following conditions.

$$v_1(1)=v_2(1), \quad v_1'(1)=v_2'(1). \tag{47}$$

The motion equations and continuity conditions can be obtained by inserting Eq. (40) into Eqs. (36), (38) and (47) in which all φ_s terms are eliminated. These yield a matrix equation which is expressed as the first column and the fourth row in matrix (42) are excluded.

$$[a_{ij}]\{b_j\}=\{0\}, \quad i=1,2,3,5,\ j=2,3,4,5. \tag{48}$$

Similarly,

$$\{b_j\}=\{C_1 \quad D_1 \quad C_2 \quad D_2\}^T. \tag{49}$$

$\det[a_{ij}]=0$ for non-trivial matrix equation gives us Eq. (44). Therefore, it is confirmed that Eq. (44) is the characteristic equation for the pure bending vibrations of two beams connected by the rigid body at their free ends. Consequently, it is expected that Eq. (45) is the characteristic equation for rotating modes of the rigid body caused by the coupled bending-torsional vibration of the beams.

6. Numerical results and system analysis

To illustrate the exactness of the induced characteristic Eqs. (44) and (45), fundamental natural frequencies from an FE model for the system and these equations are obtained by applying real values for dimensional and material parameters to them. Actually, Eqs. (44) and (45) yield normalized natural frequencies which cannot be directly compared with natural frequencies from FEM. Therefore, the following relation, which is obtained by comparing Eq. (44) with (A.15) or Eq. (45) with (A.16), is used to obtain natural frequencies.

$$\omega = \omega_n / \sigma \,, \tag{50}$$

where, ω is a natural radian frequency obtained from Eqs. (A.15) and (A.16), ω_n a normalized natural radian frequency from Eqs. (44) and (45). That is, dividing ω_n by $\sigma = \sqrt{\rho L^2 / G}$ gives us ω. In a different way, we can directly obtain ω from Eqs. (A.15) and (A.16).

The following values of the parameters are used in

Table 1. Exact solutions and FEM results for variation of d, L_0 (pure bending vibration).

unit : mm, rad./s

		L_0									
		4		6		8		10		12	
	d	Exact	FEM	Exact	FEM	Exact	FEM	Exact	FEM	Exact	FEM
ω_1	0.2	6.6	6.5	5.4	5.4	4.7	4.6	4.3	4.2	3.9	3.7
	0.4	23.8	23.8	20.3	20.3	18.0	18.0	16.3	16.3	15.0	15.0
	0.6	46.8	46.8	41.2	41.2	37.3	37.3	34.3	34.3	31.9	31.9
	0.8	72.0	72.0	65.3	65.3	60.2	60.2	56.2	56.1	52.8	52.8
	1.0	97.8	97.8	90.8	90.8	85.0	85.0	80.3	80.3	76.2	76.2
ω_2	0.2	99.3	99.2	97.7	97.7	96.5	96.5	95.5	95.5	94.6	94.5
	0.4	212.2	212.2	207.2	207.1	204.2	204.2	202.2	202.2	200.8	200.7
	0.6	339.9	339.9	328.0	328.0	320.9	320.9	316.2	316.1	312.8	312.7
	0.8	480.3	480.1	460.8	460.6	448.3	448.2	439.7	439.5	433.3	433.2
	1.0	628.6	628.4	602.9	602.7	585.2	585.0	572.3	572.1	562.5	562.3
ω_3	0.2	305.5	304.9	296.5	295.6	288.2	286.9	280.3	278.8	273.1	271.1
	0.4	648.9	648.5	639.2	638.7	632.1	631.5	626.2	625.5	620.8	620.0
	0.6	1007.8	1007.3	989.1	988.6	977.7	977.1	969.5	968.9	963.0	962.3
	0.8	1388.1	1387.1	1355.6	1354.5	1336.0	1334.8	1322.5	1321.3	1312.4	1311.1
	1.0	1787.3	1785.6	1739.6	1737.9	1709.6	1707.9	1688.7	1687.1	1673.3	1671.6
ω_4	0.2	599.2	594.2	569.3	562.3	545.5	537.2	526.8	517.8	512.1	502.8
	0.4	1315.7	1313.1	1292.0	1288.3	1271.1	1266.2	1251.6	1245.3	1233.0	1225.4
	0.6	2033.1	2030.9	2003.8	2001.3	1982.7	1979.8	1965.0	1961.7	1949.2	1945.5
	0.8	2773.1	2768.6	2728.0	2723.1	2699.3	2693.9	2677.9	2672.1	2660.4	2654.1
	1.0	3539.5	3533.0	3472.6	3466.0	3431.1	3424.4	3401.8	3394.9	3379.1	3372.1
ω_5	0.2	973.6	957.2	930.1	912.4	903.6	886.1	886.3	869.4	874.4	858.2
	0.4	2196.7	2185.4	2142.1	2125.5	2093.4	2071.7	2049.8	2023.7	2011.1	1981.6
	0.6	3409.2	3401.9	3357.7	3348.7	3314.9	3303.9	3275.9	3263.0	3239.4	3224.4
	0.8	4636.5	4622.4	4572.5	4556.3	4526.6	4508.2	4488.6	4467.9	4454.7	4431.4
	1.0	5892.2	5873.7	5804.0	5784.9	5746.6	5726.7	5702.9	5682.2	5666.6	5645.0
ω_6	0.2	1466.2	1438.3	1428.0	1401.7	1407.8	1383.0	1395.5	1371.9	1387.3	1364.6
	0.4	3280.3	3246.8	3184.4	3139.1	3108.0	3055.3	3047.8	2991.3	3000.4	2942.3
	0.6	5125.5	5105.8	5035.5	5010.1	4956.9	4925.7	4885.8	4849.2	4821.1	4779.8
	0.8	6972.2	6936.2	6877.3	6834.3	6801.8	6751.3	6735.0	6676.7	6673.3	6607.1
	1.0	8843.0	8800.0	8726.8	8681.3	8644.3	8596.0	8576.5	8525.2	8516.5	8461.9

comparing process for proving the exactness of Eqs. (44) and (45).

$$\upsilon = 0.36,\ L = 100mm,\ \rho = 8250kg/m^3,\quad E = 15GPa,\ G = E/2(1+\upsilon) \quad \text{(Beam)},$$

$$\rho_0 = 1400kg/m^3,\ b_0 = 5mm,\quad c_0 = 5mm,\ m = \rho_0 b_0 c_0 L_0 \quad \text{(Rigid body)},$$

where, υ is Poisson's ratio. The cross section of the uniform beam is assumed to be circular and its diameter is d. Therefore, the cross-sectional area, the area moment of inertia, and the polar moment of inertia are $A = \pi d^2/4$, $I = \pi d^4/64$, and $J_b = \pi d^4/32$, respectively. Especially, the distance a_1 is fixed at $c_0/2$. As the values of d, L_0 are changed, natural frequencies are calculated from computer simulation results by using a FEM program(Ansys). These are listed in Tables 1 and 2 according to their mode shapes, which are pure bending and coupled bending-torsional modes, respectively. Each mode shape is shown in Figs. 4 and 5. The results from Eqs. (44),

Table 2. Exact solutions and FEM results for variation of d, L_0 (coupled bending-torsional vibration).

unit : mm, rad./s

		L_0									
		4		6		8		10		12	
	d	Exact	FEM	Exact	FEM	Exact	FEM	Exact	FEM	Exact	FEM
ω_1	0.2	143.3	142.0	114.7	114.4	85.4	85.3	65.8	65.7	52.5	52.5
	0.4	294.8	291.7	281.2	278.4	252.9	251.3	214.0	213.3	178.5	178.2
	0.6	444.2	440.9	429.5	426.4	403.7	401.2	365.4	363.8	321.5	320.6
	0.8	593.8	587.1	576.8	569.9	548.6	542.6	508.5	504.0	460.3	457.5
	1.0	743.9	737.8	724.4	718.3	692.9	687.5	648.9	644.6	595.7	592.7
ω_2	0.2	192.9	192.5	162.0	160.4	157.4	155.6	155.9	154.0	155.0	153.1
	0.4	651.5	650.3	472.7	472.2	385.1	383.2	350.9	347.7	337.2	333.5
	0.6	1126.5	1120.8	889.2	888.1	711.8	710.9	614.9	613.1	566.3	563.6
	0.8	1555.0	1540.2	1314.0	1309.0	1073.1	1071.9	919.1	917.0	831.1	827.0
	1.0	1973.5	1958.1	1728.9	1721.3	1442.2	1439.8	1238.0	1236.2	1112.8	1109.8
ω_3	0.2	422.0	417.5	421.5	416.6	420.9	415.8	420.3	415.1	419.8	414.5
	0.4	907.3	900.1	878.4	868.9	869.6	859.3	864.3	853.7	860.5	849.7
	0.6	1600.2	1597.5	1406.6	1398.7	1362.5	1353.0	1343.5	1333.3	1331.7	1321.3
	0.8	2441.7	2438.6	2014.1	2003.2	1898.9	1881.1	1855.0	1834.4	1830.9	1808.8
	1.0	3315.8	3307.4	2674.6	2667.1	2466.2	2452.2	2389.1	2372.2	2349.5	2331.2
ω_4	0.2	820.5	811.8	820.6	811.1	820.1	810.3	819.6	809.6	819.1	809.0
	0.4	1670.9	1653.1	1669.1	1649.7	1665.8	1645.6	1662.4	1641.6	1659.2	1638.1
	0.6	2578.1	2560.1	2559.8	2540.0	2548.5	2527.8	2538.8	2517.7	2530.5	2509.0
	0.8	3565.0	3534.4	3492.3	3452.6	3465.5	3422.2	3446.9	3401.7	3431.8	3385.2
	1.0	4634.5	4609.9	4456.6	4420.5	4407.0	4367.5	4378.0	4336.9	4355.8	4313.7
ω_5	0.2	1352.7	1338.5	1352.8	1337.5	1352.5	1336.5	1351.9	1335.6	1351.5	1334.9
	0.4	2731.7	2702.1	2732.9	2700.8	2730.5	2697.2	2727.4	2693.2	2724.3	2689.5
	0.6	4149.9	4116.8	4152.1	4117.1	4146.1	4110.2	4138.0	4101.5	4130.1	4093.1
	0.8	5607.3	5541.4	5607.6	5534.8	5597.0	5520.5	5583.0	5504.3	5569.4	5488.7
	1.0	7092.8	7024.9	7088.4	7015.2	7073.8	6998.2	7055.3	6978.0	7036.1	6957.7
ω_6	0.2	2018.1	1997.1	2018.3	1995.7	2017.9	1994.4	2017.4	1993.4	2016.9	1992.5
	0.4	4061.7	4017.2	4063.8	4015.8	4061.7	4011.8	4058.6	4007.5	4055.5	4003.6
	0.6	6141.1	6088.6	6148.8	6093.7	6144.4	6088.0	6136.6	6079.4	6128.5	6070.7
	0.8	8252.2	8144.9	8270.4	8154.3	8265.1	8144.0	8252.5	8128.2	8238.4	8111.9
	1.0	10379.1	10259.1	10416.8	10291.5	10414.4	10286.2	10399.0	10268.9	10379.9	10248.4

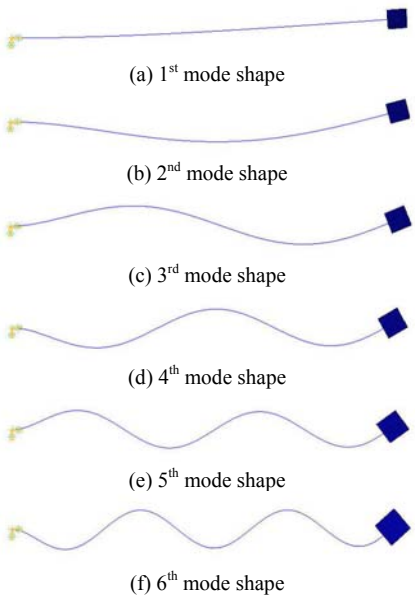

Fig. 4 Pure bending vibration mode shapes.

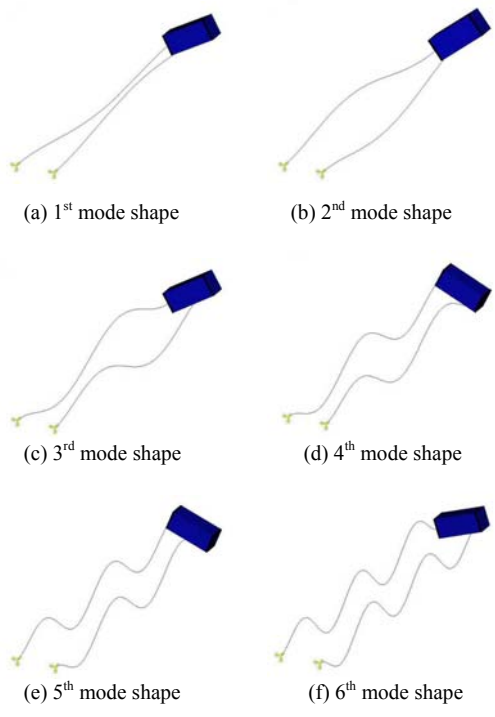

Fig. 5. Coupled bending-torsional vibration mode shapes.

(45) and (50) by using a mathematical program [19] are also listed in the same tables. As shown in the tables, the exact solutions by this study well agree with the computer simulation results. Therefore, it is clear that Eqs. (44) and (45) are the characteristic equations for the pure bending and coupled bending-torsional vibration of this system.

In addition, Eqs. (A.15) and (46) are compared. The above values for design and material parameters with $d = 0.6$ and $L_0 = 10$ are used for these calculations. The cross-sectional area and the area moment of inertia, which are twice that in Eq. (A.15), are applied to Eq. (46) because the number of beams is different in the two equations. Six natural frequencies extracted from two equations are listed in Table 3. As natural frequencies correspond exactly, it is revealed that the two characteristic equations are the same.

This paper no longer deals with the pure bending vibration characteristics because they have been analyzed by previous studies [18, 20]. From now, the coupled bending-torsional vibration characteristics by Eq. (45) are analyzed. The variations of non-dimensional parameter d/L (the ratio of the diameter to the length of the beam), L_0/L (the ratio of the width of the rigid body to the length of the beam) are applied to Eq. (45). The remaining parameters in Eq. (45) are expressed as the functions of d/L and L_0/L with given values in the above.

$$\alpha = \frac{d}{L}\sqrt{\frac{1+\upsilon}{8}}\,,\quad \zeta = \frac{1}{1+\upsilon}\,,$$
$$h = \frac{1}{\sqrt{12}}\sqrt{\left(\frac{b_0}{L}\right)^2 + \left(\frac{L_0}{L}\right)^2}\,,\quad \mu = \frac{4\rho_0 b_0 c_0}{\pi\rho L^2}\left(\frac{d}{L}\right)^{-2}\frac{L_0}{L}\,,$$
$$r = \frac{1}{2}\left(\frac{L_0}{L} - \frac{d}{L}\right). \tag{51}$$

Fig. 6(a) to 6(f) shows the variations of normalized natural frequencies with L_0/L for two values $d/L = 0.005, 0.01$. All normalized natural frequencies monotonically decrease as L_0/L increases and they converge on fixed values in the given range of L_0/L. This result implies that the mass moment of inertia of the rigid body is more largely increased than the structural stiffness and the difference of their increasing rates becomes smaller as L_0/L increases. The ratio of the first natural frequency approximately comes up to 3.5 at $L_0/L = 1$. The reduction rate gradually weakens as moving to higher natural frequency. In addition, it is discovered that the influence of the value of d/L on the variation of natural frequency becomes larger in a lower natural frequency than a higher one. In natural frequencies higher than the third one, the difference of the two curved lines is

almost proportional to that of the two values of d/L.

Fig. 7(a) to 7(f) shows the tendency of normalized natural frequency with d/L. According to the value of d/L, the variations in six natural frequencies are plotted for two values $L_0/L = 0.12, 0.36$. As can be seen, there is no doubt that the increase in d/L raises the natural frequencies. The value of L_0/L highly affects the lower natural frequency as d/L increases. The higher natural frequency is scarcely influenced by L_0/L.

It should be noted that a warping effect is added in the polar moment of inertia when a non-circular beam structure is treated.

7. Experimental results of performance

Fig. 8 shows a test actuator for experiments to be compared with the analysis in this paper. It is a small

Table 3. Comparison of mode frequency.

unit : rad./s

	ω_1	ω_2	ω_3	ω_4	ω_5	ω_6
Eq. 8	34.27	316.20	969.46	1965.02	3275.92	4885.78
Eq. 44	34.27	316.20	969.46	1965.02	3275.92	4885.78

Table 4. Comparison of resonant frequency.

	Pure bending vibration			Coupled bending-torsional vibration	
	F_1	F_2	F_3	F_1	F_2
Experiment	38	210	-	138	-
Calculation	39.6	213.3	5339.2	144.6	5339.4

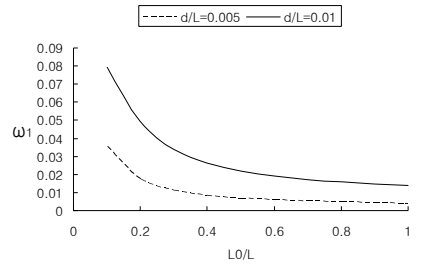

(a) Variation of 1st natural frequency

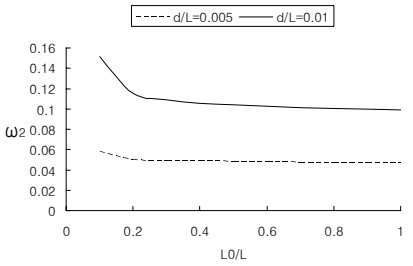

(b) Variation of 2nd natural frequency

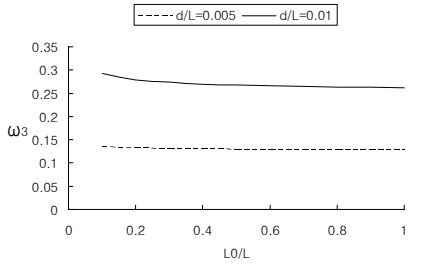

(c) Variation of 3rd natural frequency

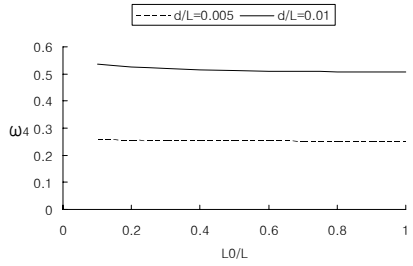

(d) Variation of 4th natural frequency

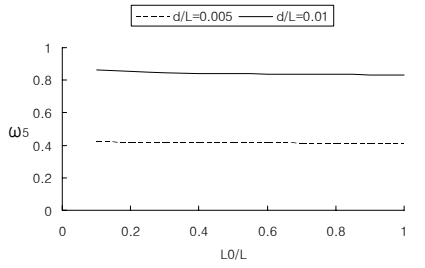

(e) Variation of 5th natural frequency

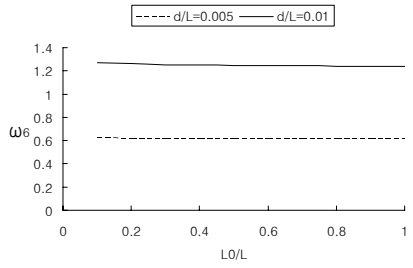

(f) Variation of 6th natural frequency

Fig. 6. Variation of natural frequency with L_0/L for two values $d/L = 0.005, 0.01$.

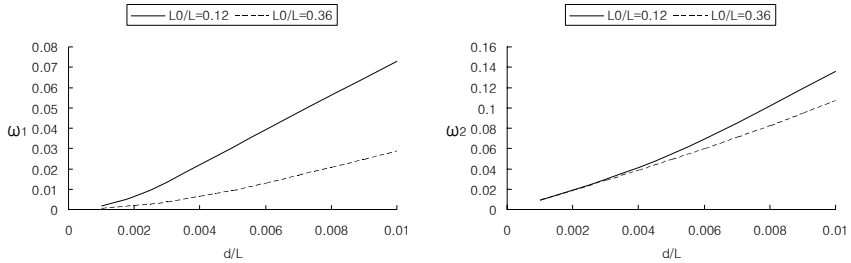

(a) Variation of 1st natural frequency

(b) Variation of 2nd natural frequency

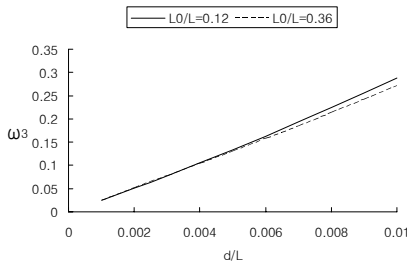

(c) Variation of 3rd natural frequency

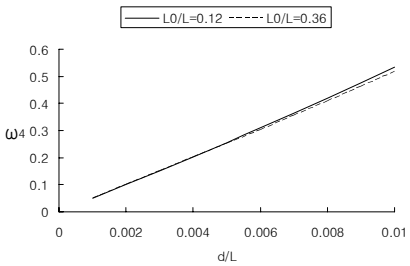

(d) Variation of 4th natural frequency

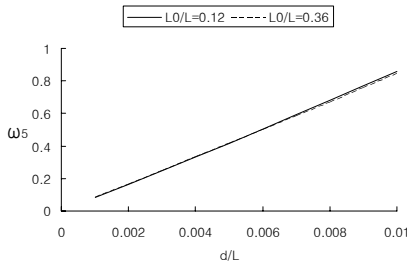

(e) Variation of 5th natural frequency

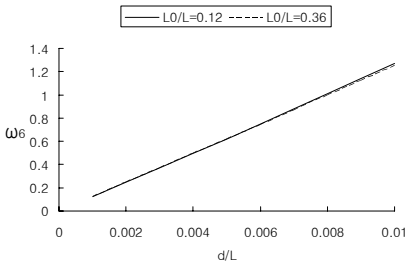

(f) Variation of 6th natural frequency

Fig. 7. Tendency of natural frequency by the variation of d/L for two values $L_0/L = 0.12, 0.36$.

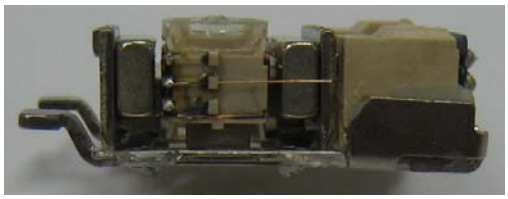

Fig. 8. Test actuator with two wire-suspensions.

and slim actuator with two wire-suspensions. The exciting force and moment are generated from voice coil motors installed in this actuator. The force moves the moving part to the lateral direction and the moment rotates the moving part around an axis parallel to the wire-suspension to obtain the lateral and rotating motions of the moving part, respectively. Mechanical values used in this test are as follows.

$$\upsilon = 0.36,\ d = 0.2mm,\ L = 11.45mm,\quad \text{(Beam)},$$
$$\rho = 8250kg/m^3,\ E = 127GPa$$
$$L_0 = 11mm,\ a_1 = 0.7mm,\ m = 0.45\times10^{-3}kg,\quad \text{(Rigid body)},$$
$$J_1 = 7.12\times10^{-9}kg\cdot m^3,\ J_2 = 5.5\times10^{-9}kg\cdot m^3$$

What has to be noticed is that m, J_1 and J_2 are not obtained from Eqs. (6) with the given material and dimensional parameters because the moving part in the test actuator is not a rectangular parallelepiped. These values are only calculated by 3-D CAD program.

Figs. 9(a) and 9(b) show frequency responses from the test actuator. Measured frequencies are compared with calculated frequencies by Eqs. (44), (45) or (A.15), (A.16) in Table 4. The first and second resonant frequencies of pure bending vibration are quite

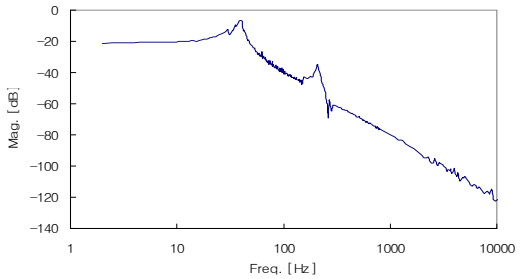

(a) Pure bending vibration

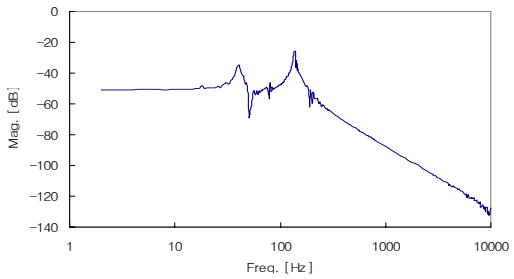

(b) Coupled bending-torsional vibration

Fig. 9. Frequency response characteristics of test actuator.

similar. The first frequency of coupled bending-torsional vibration is also similar. Other frequencies are not revealed in the experiment. In coupled bending-torsional vibration characteristics (see Fig. 9(b)), the first peak is inferred to be the first resonance of pure bending vibration because measured frequencies in two frequency response characteristics well coincide with each other. Therefore, it is concluded that the mathematical analysis is useful in the estimation of the vibration behavior of the actuator.

8. Conclusions

In order to theoretically analyze a new configuration for optical pickup actuators, the vibration of a beam structure which is composed of two beams having a rigid body at their free ends is investigated. A mathematical model, in which boundary and joint conditions are applied, yields motion equations and continuity conditions. Solving free motion problems with them gives us two characteristic equations. One is an equation for pure bending vibration of the two beams with the rigid body. The other is for their coupled bending-torsional vibration. Natural frequencies, which are obtained from these equations, are compared with the result from FE analysis, and the exactness of this study is verified. As dimensional variations are applied to the derived characteristic equation, the dynamic characteristics of this system are also analyzed. Finally, test results show that the vibration behavior of a uniform and slender beam-structure such as a new type optical pickup actuator can be simulated by this mathematical analysis.

9. references

[1] M. GURGOZE and H. BATAN, A note on the vibrations of a restrained cantilever beam carrying a heavy tip body, *Journal of Sound and Vibration* 106 (1986) 533~536.

[2] S. H. FARGHALY, Bending vibration of an axially loaded cantilever beam with an elastically mounted end mass of finite length, *Journal of Sound and Vibration* 156 (1992) 373~380.

[3] S. K. JANG and C.W. BERT, Free vibration of stepped beams: exact and numerical solutions, *Journal of Sound and Vibration* 130 (1989) 342~346.

[4] R. E. ROSSI and P.A.A. LAURA, A note on transverse vibrations of a Timoshenko beam of non-uniform thickness clamped at one end and carrying a concentrated mass at the other, *Journal of Sound and Vibration* 143(3) (1990) 491~502.

[5] N. M. AUCIELLO, Transverse vibrations of a linearly tapered cantilever beam with tip mass of rotary inertia and eccentricity, *Journal of Sound and Vibration* 194(1) (1996) 25-34.

[6] E. DOKUMACI, An exact solution for coupled bending and torsion vibrations of uniform beams having single cross-sectional symmetry, *Journal of Sound and Vibration* 119(3) (1987) 443~449.

[7] J. R. BANERJEE, Explicit frequency equation and mode shapes of a cantilever beam coupled in bending and torsion, *Journal of Sound and Vibration* 224(2) (1999) 267~281.

[8] H. GÖKDAĞ, O. KOPMAZ, Coupled bending and torsional vibration of a beam with in-span and tip attachments, *Journal of Sound and Vibration* 287 (2005) 591~610.

[9] G. L. ANDERSON, Natural frequencies of two cantilevers joined by a rigid connector at their free ends, *Journal of Sound and Vibration* 57 (1978) 403~412.

[10] H. D. KWON, Dynamic characteristics of stepped cantilever beams connected with a rigid body, *Journal of Sound and Vibration* 255 (2002)

701~717.
[11] C. A. Verschuren, F. Zijp, D. M. Bruls, J. I. Lee, J. M. A van den Eerenbeemd, K. Saito, and T. Ishimoto, Cover-layer incident near-field recording: towards 4-layer discs using dynamic tilt control, *Proc. Of SPIE,* Vol. 6282 (2006) 62820M-1~62820M-10.
[12] T. Ishimoto, S. M. Kim, A. Nakaoki, T. Kondo, Servo technologies in a near-field optical disk drive system, *Japanese Journal of Applied Physics*, Vol. 47, No. 7 (2008), 5814~5821.
[13] Y. Motegi, M. Nagasato, Y. Ishbashi, H. Someya and N. Kikuiri, Development of tilt servo system using 4-axis lens actuator for disc tilt compensation, *ISOM/ODS'99 Technical Digest, SPIE,* Vol. 3864, (1999) 20~22.
[14] Nanying He, Weipu Jia, Dingwen Yu, Lei Huang, Mali Gong, A novel type of 3-axis actuator with tilt compensation for high-density optical disc system, *Sensors and actuators A* 115 (2004) 126~132.
[15] J. M. GERE, *Mechanics of Materials*, Brooks/Cole Publishing Company, 2000.
[16] Mathematica, software version 5.0.0.0.
[17] L. MEIROVITCH, *Elements of vibration analysis*, McGraw-Hill, 1986.
[18] B. RAMA BHAT, H. WAGNER, Natural frequencies of a uniform cantilever with a tip mass slender in the axial direction, *Journal of Sound and Vibration* 45(2) (1976) 304~307.
[19] MATLAB, software version 6.5.0.
[20] R. BHAT, M. A. KULAANI, Natural frequencies for a cantilever with a slender tip mass, *American Institute of Aeronautics and Astronautics* 14 (1976) 536-537.

Appendix

For obtaining characteristic equations with dimensional parameters for solving free motion problems, the following are defined.

$$\beta^2 = \omega^2 \frac{\rho}{G}, \quad \gamma^4 = \omega^2 \frac{\rho A}{EI}, \tag{A.1}$$

$$\phi_s(x_1,t) = \phi_s(x_1)\cos\omega t, \quad v_s(x_1,t) = v_s(x_1)\cos\omega t, \quad s = 1,2, \tag{A.2}$$

where, ω is natural radian frequency. Using Eqs. (A.1) and (A.2), Eqs. (1), (2) and (16)-(20) become

$$\phi_s''(x_1) + \beta^2\phi_s(x_1) = 0, \quad s = 1,2, \tag{A.3}$$

$$v_s^{(4)}(x_1) - \gamma^4 v_s(x_1) = 0, \quad s = 1,2, \tag{A.4}$$

$$\phi_s(0) = v_s(0) = v_s'(0) = 0, \tag{A.5}$$

$$\phi_1(L) = \phi_2(L), \quad v_1'(L) = v_2'(L),$$

$$v_2(L) = v_1(L) - 2r_1\phi_1(L), \tag{A.6}$$

$$m\omega^2 v_1(L) + ma_1\omega^2 v_1'(L) - mr_1\omega^2\phi_1(L) + EIv_1'''(L) + EIv_2'''(L) = 0, \tag{A.7}$$

$$m(h_1^2 + r_1^2)\omega^2\phi_1(L) - ma_1r_1\omega^2 v_1'(L) - mr_1\omega^2 v_1(L) - 2r_1EIv_2'''(L) - GJ_b\phi_1'(L) - GJ_b\phi_2'(L) = 0, \tag{A.8}$$

$$m(k_1^2 + a_1^2)\omega^2 v_1'(L) + ma_1\omega^2 v_1(L) - ma_1r_1\omega^2\ddot{\phi}_1(L) - EIv_1''(L) - EIv_2''(L) = 0. \tag{A.9}$$

The solutions of this boundary value problem, satisfying boundary conditions (A.5), are

$$\phi_s(x_1) = B_s\sin\beta x_1, \quad s = 1,2, \tag{A.10}$$

$$v_s(x_1) = C_s(\cos\gamma x_1 - \cosh\gamma x_1) + D_s(\sin\gamma x_1 - \sinh\gamma x_1), \quad s = 1,2. \tag{A.11}$$

$B_1 = B_2$ is apparent by the first boundary condition $\phi_1(L) = \phi_2(L)$ in Eq. (A.6). Inserting Eqs. (A.10) and (A.11) into Eqs. (A.6)-(A.9) gives the following matrix form.

$$\left[a_{ij}\right]\left\{b_j\right\} = \left\{0\right\}, \quad i,j = 1,2,3,4,5. \tag{A.12}$$

The components of matrix $\left[a_{ij}\right]$ are as follows.

$$\begin{aligned}
&a_{11} = 0, \quad a_{12} = s + sh, \quad a_{13} = -(c - ch),\\
&a_{14} = -(s + sh), \quad a_{15} = c - ch,\\
&a_{21} = 2r_1\sin\beta L, \quad a_{22} = -(c - ch),\\
&a_{23} = -(s - sh), \; a_{24} = c - ch, \quad a_{25} = s - sh,\\
&a_{31} = mr_1\omega^2\sin\beta L,\\
&a_{31} = mr_1\omega^2\sin\beta L\\
&a_{32} = -m\omega^2(c - ch) + ma_1\omega^2\gamma(s + sh), - EI\gamma^3(s - sh)\\
&a_{33} = -m\omega^2(s - sh) - ma_1\omega^2\gamma(c - ch) + EI\gamma^3(c + ch),\\
&a_{34} = -EI\gamma^3(s - sh), \quad a_{35} = EI\gamma^3(c + ch),\\
&a_{41} = -m(h_1^2 + r_1^2)\omega^2\sin\beta L + 2GJ_b\beta\cos\beta L,\\
&a_{42} = -ma_1r_1\omega^2\gamma(s + sh) + mr_1\omega^2(c - ch),\\
&a_{43} = ma_1r_1\omega^2\gamma(c - ch) + mr_1\omega^2(s - sh),\\
&a_{44} = 2r_1EI\gamma^3(s - sh), \quad a_{45} = -2r_1EI\gamma^3(c + ch),\\
&a_{51} = ma_1r_1\omega^2\sin\beta L,
\end{aligned} \tag{A.13}$$

$$a_{52} = m(k_1^2 + a_1^2)\omega^2\gamma(s + sh) - ma_1\omega^2(c - ch) - EI\gamma^2(c + ch)$$
$$a_{53} = -m(k_1^2 + a_1^2)\omega^2\gamma(c - ch) - ma_1\omega^2(s - sh) - EI\gamma^2(s + sh)$$
$$a_{54} = -EI\gamma^2(c + ch), \quad a_{55} = -EI\gamma^2(s + sh),$$

where, $s + sh = \sin\gamma L + \sinh\gamma L$, $s - sh = \sin\gamma L - \sinh\gamma L$, $c + ch = \cos\gamma L + \cosh\gamma L$, and $c - ch = \cos\gamma L - \cosh\gamma L$. Modal vector is

$$\{b_j\} = \{B_1 \quad C_1 \quad D_1 \quad C_2 \quad D_2\}^T. \tag{A.14}$$

From $\det[a_{ij}] = 0$ for non-trivial solution, characteristic equations are obtained.

$$(k_1^2 m^2\omega^4 + 4E^2I^2\gamma^4) - [(k_1^2 m^2\omega^4 - 4E^2I^2\gamma^4)\cos\gamma L + 2mEI\gamma\omega^2(a_1^2\gamma^2 + k_1^2\gamma^2 + 1)\sin\gamma L]\cosh\gamma L - 2mEI\gamma\omega^2[(a_1^2\gamma^2 + k_1^2\gamma^2 - 1)\cos\gamma L + 2a_1\gamma\sin\gamma L]\sinh\gamma L = 0, \tag{A.15}$$

$$(2\beta GJ_b\cos\beta L - h_1^2 m\omega^2\sin\beta L)(1 - \cos\gamma L\cosh\gamma L) + 2EI\gamma^3 r_1^2\sin\beta L(\sin\gamma L\cosh\gamma L + \cos\gamma L\sinh\gamma L) = 0. \tag{A.16}$$

As explained in chapters 5 and 6, Eqs. (A.15) and (A.16) are the characteristic equations for the pure bending and coupled bending-torsional vibrations of two beams caused by joint condition at their free ends.

Kyung Taek Lee received a Ph.D. degree in Mechanical Engineering from Yonsei University, Seoul, Korea in 2003. He joined LG Electronics, Seoul, Korea, in 1989, where he has worked on precise mechanical structures and microactuating systems for optical information storage devices, as a Research Engineer. His current interests include microactuators for position control, haptic elements for mobile devices, and etc.